Determination of the ionization and acceleration zones in a stationary plasma thruster by optical spectroscopy study: Experiments and model

N. Dorval, J. Bonnet, J. P. Marque, et al.

View Online

Export Citation

ARTICLES YOU MAY BE INTERESTED IN

Determination of the ionization and acceleration zones in a stationary plasma thruster by optical spectroscopy study: Experiments and model

N. Dorval, J. Bonnet, J. P. Marque and E. Rosencher[a]
ONERA/DMPH, Chemin de la Hunière, 91761 Palaiseau, France

S. Chable and F. Rogier
ONERA/CERT/DTIM, Toulouse, France

P. Lasgorceix
*Laboratoire d'Aérothermique du CNRS, 1C avenue de la Recherche Scientifique,
45071 Orléans Cedex 2, France*

A stationary plasma thruster is experimentally studied using different optical spectroscopies of xenon ions. Doppler shift in laser induced fluorescence is used for velocity determination while the ion density is determined by emission spectroscopy. These experiments show unambiguously that the ionization and the acceleration zones are spatially distinct inside the thruster channel. Moreover, it is shown that these results can be easily taken into account with a very simple quasineutral stationary one-dimensional model. © *2002 American Institute of Physics.*
[DOI: 10.1063/1.1458053]

I. INTRODUCTION

Thanks to their high specific impulses and high thrust efficiency, Hall thruster or stationary plasma thrusters (SPTs) are currently envisaged for commercial, extraplanetary and military space missions. These devices have been mostly developed by Russian teams in the early 1970s.[1] One of the main advantages of SPT compared to electrostatic ion thrusters is that the ion accelerating cathode is virtual, localized near the magnetic field maximum, where the electron mobility is decreased due to the electrons being trapped on Larmor orbits. On the other hand, in electrostatic ion thrusters, the grid cathode is placed in view of the ions and is thus submitted to sputtering, leading to potentially shorter lifetimes.

Knowledge of the physical processes involved in SPT needs modeling along with its validation by dedicated diagnostic tools. *In situ* optical methods turned out to be very powerful tools for a nondisturbing and sensitive analysis of plasma flows. Laser induced fluorescence (LIF) spectroscopy is well suited for probing the species produced in SPT such as xenon ions, Xe^+ and measuring their velocities with both selectivity and high spatial resolution. This technique has already been used to investigate Hall-type thrusters. Let us cite here the works of Manzella[2] and of Hargus and Cappelli[3] who used the $5d[4]_{7/2}-6p[3]_{5/2}$ singly ionized xenon excitation transition at 834.7 nm to map the velocity vectors in the plume of a SPT- 100 plume for the former, and of a laboratory Hall thruster, for the latter. Hargus and Cappelli have also measured the axial velocity of ionic xenon inside the channel and found that significant acceleration ($>60\%$) occurred outside the channel.

In this article, we present LIF together with plasma emission experiments inside and outside the channel of a laboratory SPT-100 ML plasma thruster. We report on the measured axial profiles of $Xe^+ 5d[4]_{7/2}$ axial velocity and of $Xe^+ 6p[3]_{5/2}$ emission at 541.9 nm. We unambiguously demonstrate that ionization and acceleration occur in two different zones of the SPT. Then, we show that the experimental results agree satisfactorily well with a very simple heuristic one-dimensional (1D) computational model.

II. EXPERIMENTAL SETUP

The experiment took place in the "PIVOINE" facility of the Laboratoire d'Aérothermique du CNRS with the SPT 100-ML model built within a SNECMA/CNRS/CNES collaboration. This facility and the SPT 100 ML are described in detail in Ref. 4. The test facility consists of a vacuum chamber (2.2 m in diameter, 4 m in length) with a cryogenic pumping system (pumping speed of 70 000 l/s). The thruster is fed with 5 mg s^{-1} of xenon (99.9995% pure) through the anode which yields a tank pressure of 2.7×10^{-5} mbar. It operates under the following conditions: discharge voltage $=300$ V, discharge current$=4.25$ A, magnetic coil current $=4.5$ A. Under these conditions, the thruster is working in a fluctuating current mode.[4]

An external-cavity diode tunable laser centered at 834.7 nm (SDL TC-10) is used to excite the Xe^+ ions from $5d[4]_{7/2}$ to $6p[3]_{5/2}$ states. Its main features are: continuous wave, single-mode, output power of 14 mW (for an operating current of 65 mA and a cavity temperature regulated at 25 °C), instantaneous linewidth below 200 kHz, jitter <2 MHz for an averaging time over 10 s. Fine tuning range without mode hops over 60 GHz is achieved by adjusting the voltage applied to the piezoelectric actuator. In practice, it is finely tuned over 32 GHz to capture the Doppler shift from the excitation spectrum of high speed ions (i.e., up to ~20 km/s). Laser emission wave number is measured by means of a four Fizeau interferometer device (model LM-
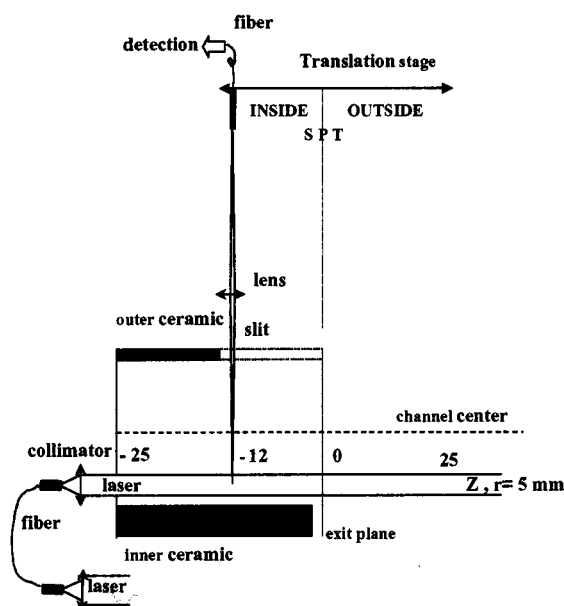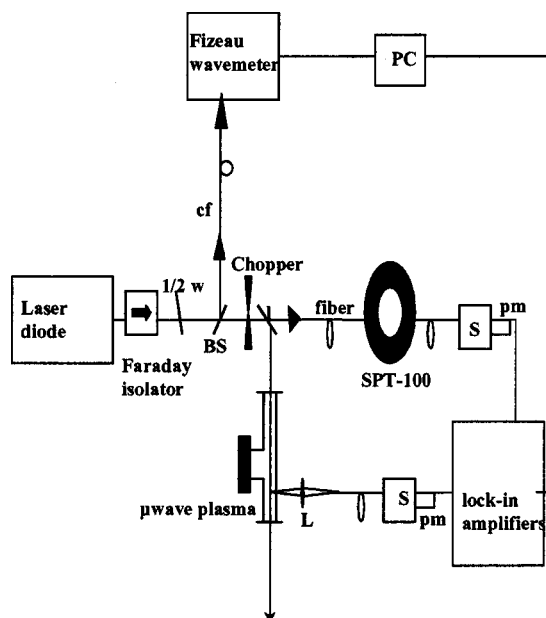
FIG. 1. Layout of laser induced fluorescence apparatus: $\frac{1}{2}$ w : achromatic half wave plate (500–800 nm); BS : beam splitter cube (650–900 nm) with $T=85\%$ for p polarization; l : beam splitter plate with $T=60\%$ @ 45° and for p polarization; L: lens $f=40$ mm, $D=20$ mm, $G=1$; cf: fiberoptic coupler; S: spectrograph Jobin–Yvon H20 visible equipped with a 0.5-mm-wide slit at the exit (bandpass of 2 nm); pm: photomultiplier tube RCA (a). Layout of laser beam path and fluorescence collection in SPT (b).

FIG. 2. Axial profile of the radial magnetic field measured by Hall probes

007 supplied by Laser 2000) with a precision of ± 0.003 cm^{-1}. A 2.45 GHz surface wave plasma of xenon (pressure of 0.3 Pa, incident power of 50 W) is used as a zero-velocity ion source. It enables a straightforward measurement of Doppler shifts of the spectra of the Xe$^+$ ions ejected from the SPT [see Fig. 1(a)].

After passing through a Faraday isolator and a mechanical chopper, the laser beam is coupled into a multi-mode fiber of 50 μm core and 20 m long. At the output of the fiber, the beam is collimated (3 mm in diameter) and enters the SPT by passing through a pinhole made in the rear of the
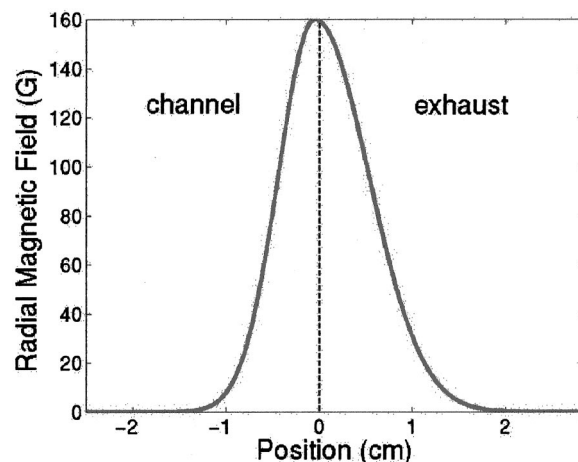
channel. It is propagated along the thruster axis—in the ion beam propagation direction—to allow measurements of axial component of velocity. The laser axis is close to the inner ceramic wall of the channel. Radial location in the channel is 5 mm from the inner ceramic wall [see Fig. 1(b)].

The fluorescence light at 541.9 nm is collected at 90° from the laser axis—outside the channel as well as inside the channel through a 15-mm-long and 2-mm-wide slit drilled in the outer ceramic wall—by means of a lens (11 mm in diameter, 25 mm focal length) coupled to a movable optical fiber (200 μm in diameter). The laser intensity is roughly 600 μW/mm^2 in the probe volume of 0.2 mm long. Measurement is performed at several axial locations from inside to outside the channel with a minimum step of 0.5 mm in the vicinity of the exit plane. Negative position z<0 (respectively, positive one $z>0$) indicates location inside (respectively, outside) the exit plane of the SPT channel taken as the reference position, $z=0$ [see Fig. 1(b)]. Velocity is measured with a precision lying between ± 100 and ± 800 ms^{-1}. (The worst values are due to a significant broadening of the spectrum within a thin layer upstream from the exit plane.) Finally, the magnetic field distribution along the channel axis (see Fig. 2) is determined by a Hall probe, the displacement of which is computer controlled.

Figure 3(a) shows the excitation spectra of Xe$^+$ which are observed from 2 to 25 mm outside the exit plane, together with the one *simultaneously* measured in the zero-velocity reference plasma source (in dotted line). We clearly see the variation of the Doppler shift as well as of the width of the spectrum as a function of the axial location.

Going inside the channel (i.e., $+2$ to -1 mm), one observes a progressive broadening of the spectra which is clearly seen on the normalized curves of Fig. 3(b). It is worth noting that an almost twofold broadening of the spectrum occurs within 1.5 mm in the zone located between 0.5 and 2 mm inside the channel which strongly affects the precision of velocity measurement, i.e., from ± 100 to 800 ms^{-1}. Also, the signal to noise ratio drops by a factor 3. There is also the appearance of evenly spaced peaks in the spectrum (500–700 MHz) clearly seen in Fig. 3(c). This striking change is likely to arise from plasma oscillations or instabili-
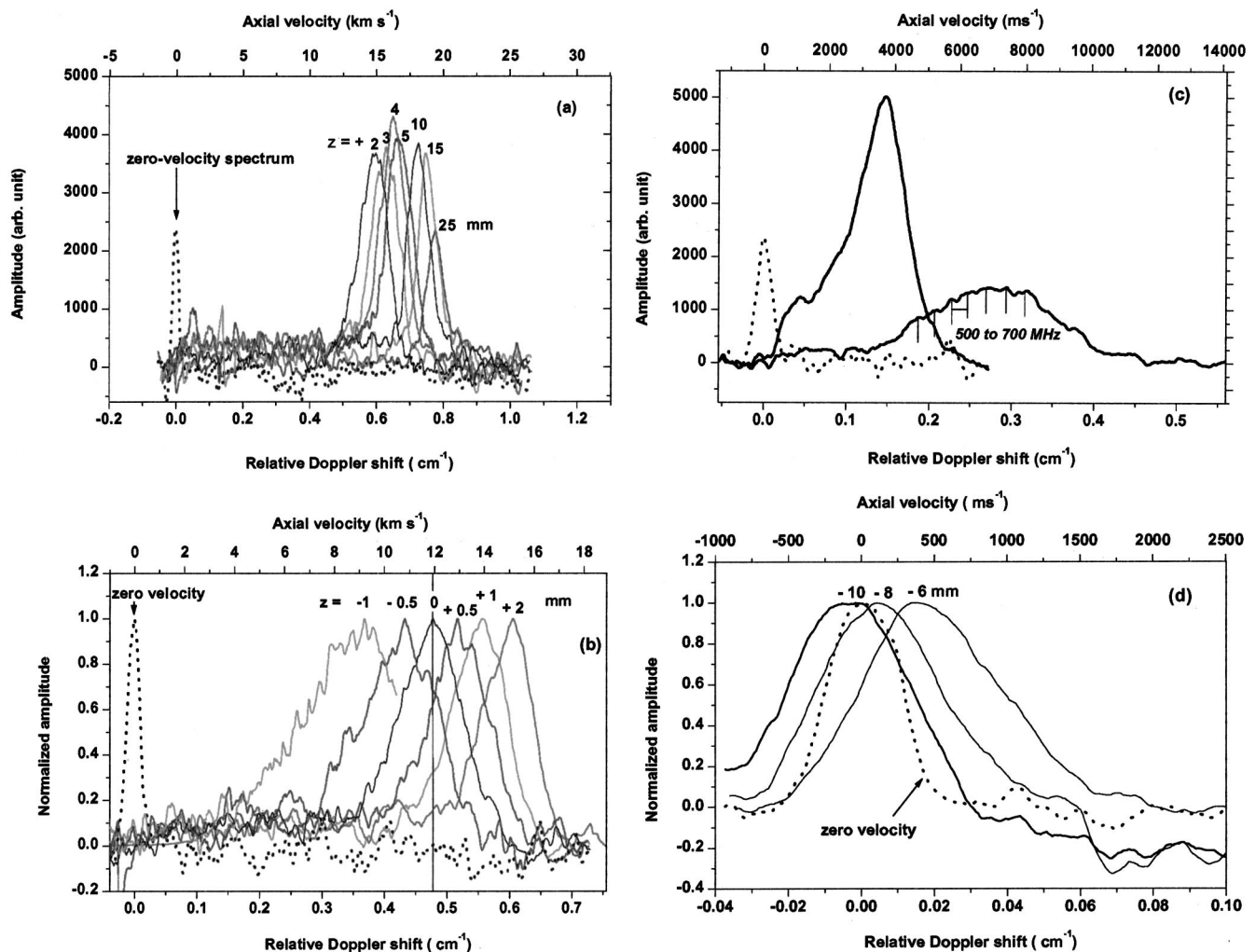
FIG. 3. The $5d[4]_{7/2} - 6p[3]_{5/2}$ Doppler-shifted excitation spectra of the Xe^+ ions recorded at various axial positions outside the channel at a radial location of 5 mm from the center of the channel. The zero-velocity spectrum which is recorded *simultaneously* in the reference microwave plasma is shown in dotted line. (a) Spectra recorded close to the exit plane (b). Evenly spaced peaks (500–700 MHz) observed at −0.5 mm inside de channel (c). Spectra observed from 6 to 10 mm inside the channel (d). Distances are relative to the exit plane, $z=0$ taken as the reference position.

ties but it has to be asserted by spectral simulation which could account for such effects. Finally, deeper inside the channel [see Fig. 3(d)], the Doppler shift vanishes, showing that ions are not yet accelerated and the spectrum width narrows to a minimum value of 1.3 GHz [though it is always wider than the one recorded simultaneously in the microwave plasma in a dotted line, i.e., full width at half maximum (FWHM) of ~700 MHz]. The interpretation of the spectrum shape and its exploitation to infer additional data such as velocity dispersion (or kinetic temperature), should require the simulation of the hyperfine, isotopic and (possibly) Zeeman structures of the transition $5d[4]_{7/2} - 6p[3]_{5/2}$ of Xe^+.

Figure 4 shows the spatial evolution of the ion velocity deduced from the Doppler shift measurements. One clearly observes that most of the acceleration ($>80\%$) occurs from −2.5 to +2.5 cm. Moreover, in accordance with Hargus and Cappelli's results, a significant portion of the ion acceleration is obtained outside the SPT channel, i.e., away from the magnetic field maximum. This will be discussed later.

Using the same detection apparatus, we have measured the $Xe^+ 6p[3]_{5/2}$ emission at 541.9 nm induced by the plasma in the same working conditions, as a function of axial location. We assume that the quantity of 541.9 nm light emitted by the $Xe^+ 6p[3]_{5/2}$ ions is proportional to the plasma density. Figure 5 shows the emission signal induced by the plasma together with the ion velocity distribution of Fig. 4. This figure confirms the main mechanisms which are at stake in the SPT channel in nominal thrust conditions. The maximum plasma density is situated in an *ionization region* which, by definition, is the region where the ion density and ionization rate are (almost simultaneously) maximum. For nominal working conditions, this ionization zone is situated inside the SPT channel. The ions are then accelerated by the electric field which increases dramatically in the region of maximum magnetic field in order to compensate the decrease of the mobility of the electrons trapped on their Larmor orbits. This will be confirmed by the numerical model below. Let us note finally the exponential decrease of the plasma density towards the anode.
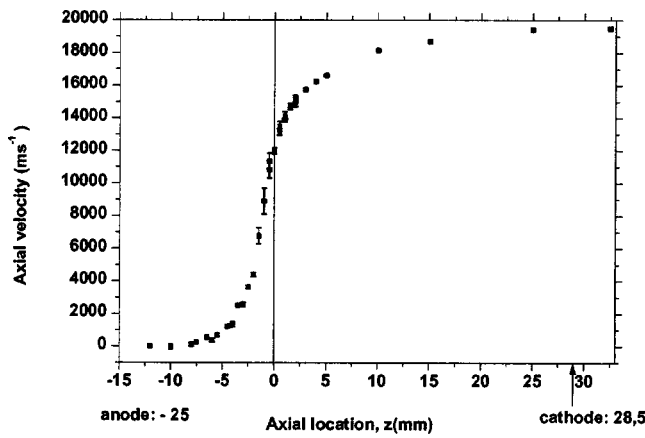
FIG. 4. Axial velocity determined from Doppler shift as a function of the axial location in the thruster.

FIG. 6. Axial profile of the electric field derived from data of Fig. 4

In order to have a closer look at this *acceleration zone*, we first calculate the kinetic energy E_c of the Xe^+ ions from data of Fig. 4. The electric field is then determined by the spatial derivation of this kinetic energy dE_c/dz. Let us note that this latter calculation is valid for two conditions: (i) the ion transport is ballistic (which is an excellent approximation), (ii) the Doppler line shape is not too disturbed so that the maximum of the line shape still reflects the ion mean velocity. This latter condition is more questionable and is the subject of present investigations. The results are shown in Fig. 6. We find that the acceleration zone is peaked at 1 mm in the channel with a maximum electric field of 460 V/cm where the radial magnetic field is maximum. This acceleration zone is rather thin since the full width at half maximum (FWHM) is less than 2 mm wide but it extends deeply into the plume since significant electric field (50 V/cm) is still reigning 10 mm away from the SPT exit.

III. NUMERICAL MODEL

Our experimental results are now analyzed with the support of a plasma model which is specific by its simplicity. Indeed, many detailed models have been already proposed in
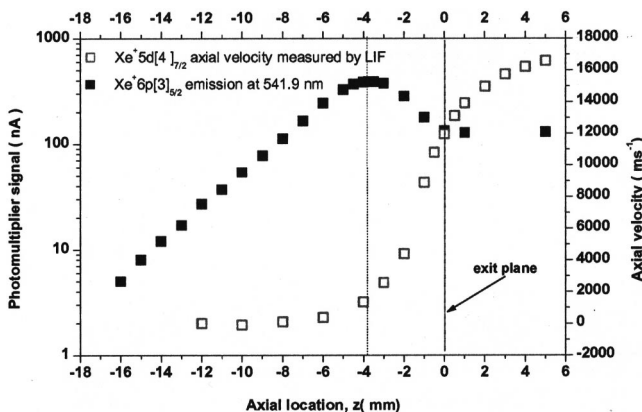

FIG. 5. Comparison between the axial profiles of the axial ion velocity and of the 541.9 nm $Xe^+6p[3]_{5/2}$ emission. Considering that the emission intensity is proportional to the ion density, the figure shows evidence of the existence of two zones related to distinct physical phenomena, viz., ionization and acceleration.
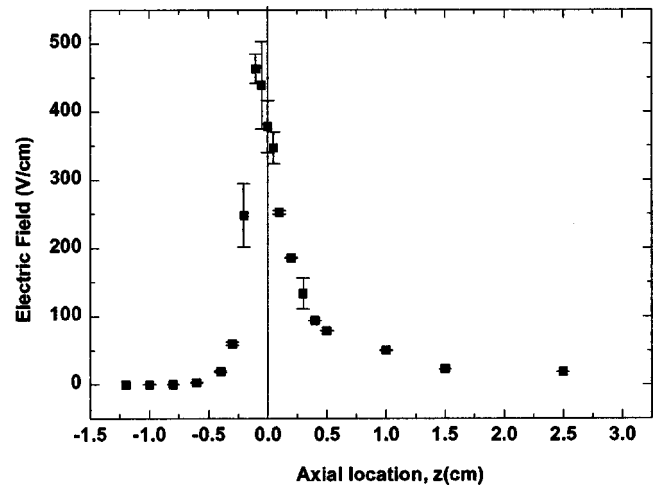
the literature for the study of SPT plasmas. Fife, Matinez-Sanchez, and Szabo[5] described a two-dimensional (2D), non quasineutral model which assumed that electrons obey a Maxwellian distribution and heavy particles are kinetics. These particle-in-cell simulations[6] agree with SPT-70 experimental data and effectively display the experimentally observed oscillations. In 1998, Garrigues and Bœuf[10] proposed a simple, quasineutral, hybrid fluid nonstationary 1(D) model. The numerical results compare well with the experimental data and, for instance, display the experimentally observed low-frequency oscillations. For the study of the SPT plume, Van Gilder and Boyd[7] developed a non quasineutral approach, assuming a Boltzmann law for the electrons, and using a direct Monte Carlo simulation in order to treat collisions accurately. Finally, Bareilles, Garrigues, and Bœuf,[8] using a rather similar approach but with a simple, treatment for the collisions, obtained numerical ion current distribution which is in very good agreement with the experiments. The basis of our approach is to write a very simple model derived from the Garrigues–Boeuf model[10] in order to specifically address the main points covered by our experiments: (i) the residual acceleration observed outside the channel and (ii) the two different zones (i.e., ionization and acceleration) observed in the channel. To reach this goal, as we will show now, a very crude stationary one-dimensional modeling is indeed sufficient.

The main assumptions of this model are recalled now: the electrons are approximated by a Maxwellian fluid, the heavy particles are ballistic, the magnetic field (supposed only radial) is only due to the external magnetic coils while the one induced from the current through the SPT is neglected (i.e., not self-consistent), the electronic mobility includes the electron wall collisions, ions are not sensitive to the magnetic field and the neutral Xe velocity is spatially constant. The model is extended outside the channel to the cathode taking into account the magnetic field distribution outside the channel. We assume that the electric potential is monotonically decreasing; this assumption imposes an *a priori* estimation on the electric potential which is not restrictive. By solving the Vlasov equations, we obtain the ion and

neutral densities as a function of the electric potential as

$$n_i(z) = \frac{N_i^0 v_0}{\sqrt{v_0^2 + 2\frac{e}{m_i}[U - \phi(z)]}}$$

$$+ \int_0^z \frac{k_i n_0 n_i(y)}{\sqrt{v_0^2 + 2\frac{e}{m_i}[\phi(y) - \phi(z)]}} dy, \qquad (1)$$

$$n_0(z) = N_0^0 \exp\left(-\int_0^z \frac{k_i n_i(y)}{v_0} dy\right), \qquad (2)$$

where ϕ, n_i and n_0 are, respectively, the electric potential, ion and neutral densities, U, N_i^0, N_0^0 are their values at the anode. The electric potential is supposed to be equal to 0 at the cathode. The term v_0 is the neutral velocity, k_i is the ionization rate which depends on the mean electronic energy ϵ. It is deduced from the model of Ref. 9: a steady state mean energy equation is considered. Only single ionization is included in the model.

A nontrivial point consists of the treatment of the plasma interaction with the insulator wall. Since an electron impacting a solid surface may be scattered back, a proportion of its energy is transferred to secondary electrons. This mechanism represents a significant energy loss at temperatures around 30 eV for which the emission coefficient for secondary electrons approaches 1. Garrigues and Boeuf[10] take into account the electron-wall interactions by including an electron-wall momentum exchange frequency α and an electron-wall energy exchange frequency which takes the simple form: $\alpha \exp(-(U/\epsilon))$ where U is a constant Debye sheath voltage and ϵ is the electron mean energy. This expression is deduced from the assumption of an electron Boltzmann distribution. The term α is proportional to the electron thermal velocity and inversely proportional to the distance between the two radii. The results obtained are not sensitive to the variation of the wall potential.

Outside the channel, in order to avoid a nonphysical singularity in the energy profile, the wall-electron interactions are smoothly faded to zero at 1.5 cm from the exhaust. This fading term allows the electron to drift away from this region where the magnetic field is still large enough to trap them on Larmor orbits. It is most likely that this heuristic term stems physically from 2D effects which are not described by this simple approach (radial gradient of the magnetic and electric fields). Other approaches have been tried such as introducing a Bohm diffusion term[11,12] to explain the presence of anomalous cross-field electron mobility but the results were not convincing. This fading term is currently investigated by 2D simulations.

The electron density is deduced from the quasineutrality condition. The electron momentum equation is supposed to take the simple form: $v_e = -\mu E$, where μ is the classical electron mobility in a transverse magnetic field[12]

$$\mu(z) = \frac{e}{m_e \nu(z)} \frac{1}{1 + (\omega_B^2/\nu^2)(z)}, \qquad (3)$$

where ω_B is the cyclotron frequency. The collision frequency ν is given by $\nu(z) = \nu_m(z) + \nu_w$ which takes into account the electron-wall interactions $\nu_w = 0.2 \times 10^7$ cm^{-1} and the electron-neutral collisions $\nu_m(z) = k_m n_0(z)$ with $k_m = 2.5 \times 10^{-7}$ cm^3 s^{-1}. The displacement current is neglected and the electric field is resolved using the current continuity (see Ref. 10 for more details).

For the heavy particles transport equation, we approximate the integrals by middle point quadrature. The positivity of n_{0l} and n_{il} is assured under the stability condition $\Delta z \leq 2v_0/k_{ij}n_{0j}$. The electron energy equation is nonlinear (electrons-wall interaction) and is integrated with a fourth order Runge–Kutta method. In order to solve the potential equation, we use a second order scheme. Ion density, neutral density, electric potential and mean electron energy are successively calculated until ion density converges. An over relaxation method is used to solve densities and energy. It means that electron energy converges faster than densities.

Clearly, plasma oscillations cannot be predicted by this stationary approach but the simulation outputs are in excellent agreement with the time averaged Garrigues and Bœuf ones. On the positive side, the computational cost is very low: it only requires the resolution of an ordinary differential equation system. For instance, using a 400 cell mesh, the numerical simulation takes 1 min on a 440 MHz workstation.

IV. RESULTS AND DISCUSSION

We discuss now the resulting axial profiles of the plasma parameters. We take the physical parameters of SPT-100 ML as:

(1) column voltage of 300 V,
(2) a mass flow rate of 5 mg/s; and
(3) an axial profile of the magnetic field experimentally determined by Hall probes (see Fig. 2). A peak of 160 G is measured close to the channel exit and decreases steeply outside the channel.

For some values of the applied voltage (>400 V see Ref. 4), the SPT is known to display oscillations. We have checked that, for cases with oscillations, the time averaged profiles of our stationary model are similar to the profiles of the nonstationary model. This justifies the use of our stationary approach which leads to far smaller computational time than the nonstationary one. Figures 7(a), 7(b), 7(c), 7(d), 7(e), and 7(f) show, respectively, the electric field, mean electron energy, electron mobility, neutral density, axial ion velocity and ion density. In Fig. 7(a), it appears that the electric field maximum occurs inside the channel close to the exit plane where the radial magnetic field reaches its maximum value: this zone, named the "acceleration zone," is the zone where the ions are accelerated and extracted from the plasma. This is indeed the basic principle of SPT in action since the electric field in the large magnetic field region increases in order to compensate for the low electron conductivity and to ensure current continuity. In other words, the electric field is roughly inversely proportional to the mobility, i.e., proportional to the square of the magnetic field through Eq. (3). This is confirmed in Fig. 7(c) which shows
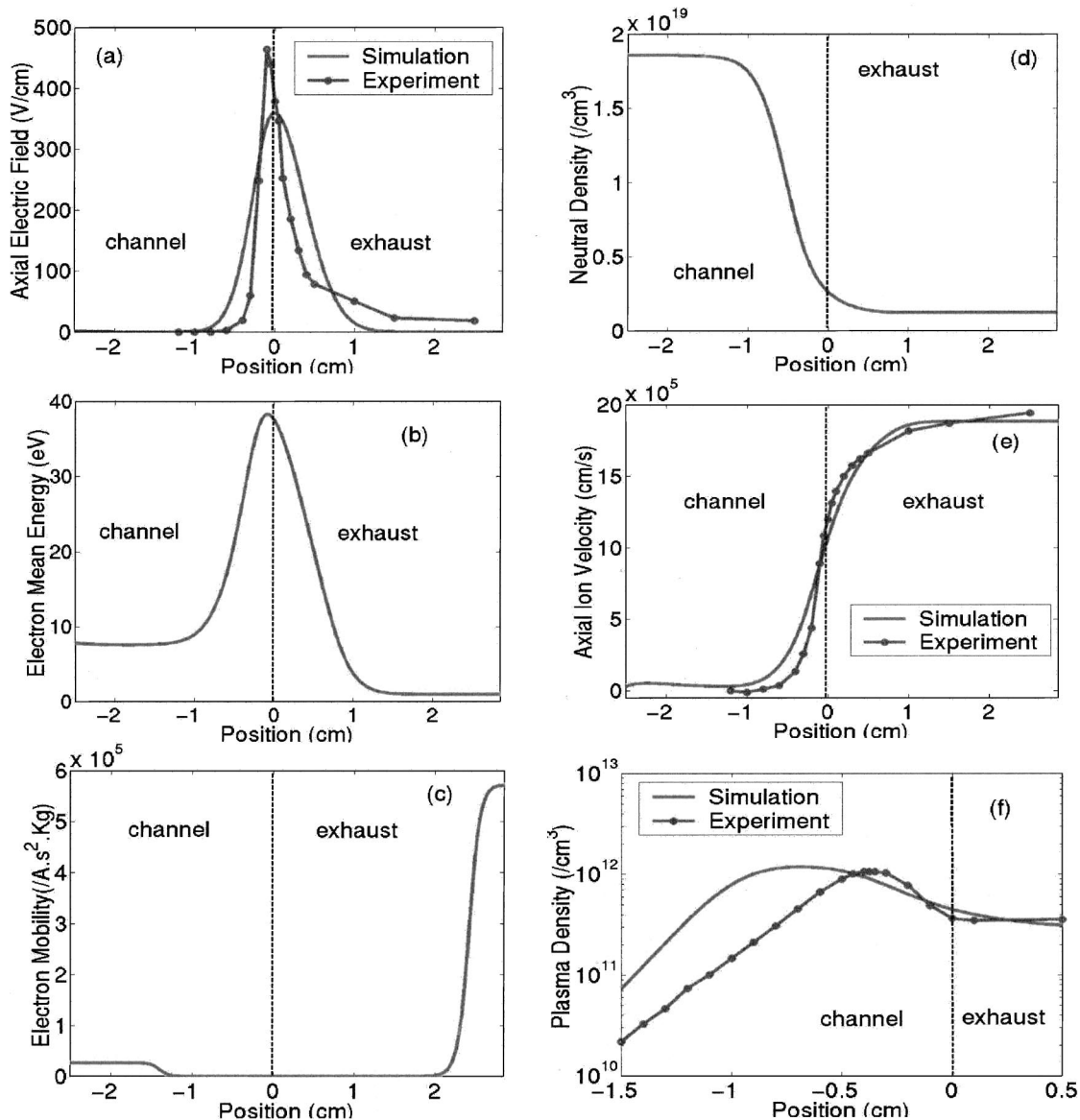
FIG. 7. Comparison between the experimental and the calculated electric field distributions (a). Calculated mean electron energy (b). Calculated electron mobility (c). Calculated neutral density (d). Comparison between experimental and calculated axial ion velocity vs axial location (e). Calculated plasma density and experimental $Xe^+ 6p[3]_{5/2}$ plasma emission vs axial location (f).

the electron mobility: in the low magnetic field region, the electron mobility is indeed large while, in the large magnetic field region, the electrons are confined on their Larmor orbits and only the electron-neutral and electron-wall collisions are allowing them to drift toward the anode. In Fig. 7(b), the electron mean energy is found to be maximum close to the exit channel and decreases in the low electric field regions. Outside the channel, it remains constant to a value which can be taken as a parameter. We have chosen a value of 1 eV in order to prevent Xe numerical ionization outside the channel by the Maxwellian tail of the electron distribution. Indeed, taking a larger limit condition of 10 eV yields numerical ionization of Xe which is not observed experimentally. Figure (7f) shows that the plasma density reaches a value of 1.2 10^{12} cm^{-3} at a distance of 0.5 cm inside the channel. Outside the channel, the ion density slightly decreases because it is just accelerated by the electric field: they are not colli-

sional and become ballistic. This is in contrast with Fig. 7(d) where the neutral density is shown to be constant from the anode to 1.75 cm from the exit and decreases to reach about 10% of its anode value due to ionization. The transition region where most of the ionization takes place is also named ''production zone'' or ''ionization zone.''

Figure 7(e) compares the axial ion velocity determined by the LIF measurements and the result of the model. In spite of the crudeness of our heuristic model and the two-dimensional effects which take place inside and outside the channel—the magnetic field lines are strongly curved—the agreement is rather satisfactory. The ion velocity increases to reach in the exhaust about 12 000 m s^{-1}. Outside the channel, it is almost constant and equal at 19 500 m s^{-1}. In quadratic norm, there is an error of 7% between the experiment and the model. Finally, Fig. 7(f) shows the calculated plasma density. This overall profile agrees rather well with the ex-

perimental axial profile of the $Xe^+ 6p[3]_{5/2}$ plasma emission of Fig. 5 [shown again in Fig. 7(f)]: there is effectively an exponential increase of the plasma density from the anode and the plasma density varies only slightly in the acceleration zone. However, there is an important discrepancy between the experimental curve and the numerical model output. For instance, in the exponential increase region (between 2 and 0.5 cm from the exhaust), the theoretical gradient is 25% larger than the experimental one. The reasons for this discrepancy are still unclear: it might stem from (i) 2D effects in a region where the radial component of the magnetic field becomes important or (ii) a nonlinear relationship between the excited levels population and the plasma density due to the variation of the electronic temperature along the channel axis.[13]

The ion current is calculated to be about 3.85 A at the cathode. It corresponds to a thrust of about 0.094 N and a specific impulse of 1913 s. This is in good agreement with experimental results: for the same working conditions (discharge voltage 300 V, 5 mg/s xenon flow), the measured thrust is 86.3 mN and the specific impulse is 1759 s.[14] In the presented experiments, the thrust calculated from the experimental axial ion velocity is 0.098 N, neglecting the divergence of the ion beam. Finally, let us note that, in agreement with previous authors (for instance, Meezan, Hargus, and Cappelli[11]), the wall mobility approach seems efficient to explain the experimentally observed anomalous conductivity. Moreover, the heuristic decrease of the wall mobility term outside the channel, though it cannot be physically justified, is sufficient to obtain realistic and reliable numerical results.

V. CONCLUSIONS

Optical spectroscopy measurements have unambiguously displayed two different regions in the SPT thruster.

(1) An ionization zone where most of the plasma is created and where the $Xe^+ 6p[3]_{5/2}$ emission at 541.9 nm is maximum. In this region, the magnetic field is small, the electron mobility is thus high and correlatively the electric field is small. The electron energy is then small enough to meet the maximum of the Xe ionization yield.

(2) An acceleration zone where the $5d[4]_{7/2} - 6p[3]_{5/2}$ singly ionized xenon transition is maximum. In this region, the magnetic field is high, the electron mobility is low, the electric field is high for achieving current continuity and, consequently, the ions are highly accelerated. The half width at half maximum of this high field region profile is extremely thin, i.e., in the 2 mm. However, an important part of the ion acceleration takes place outside the SPT channel, where the magnetic field is still high. Because of the radial component of this magnetic field, the acceleration is divergent, which is confirmed by experiments. In order to reduce the plume divergence, a good idea is to improve the magnetic field topology at the exit part of accelerating,[15] which calls for a real 2D model.

The one-dimensional quasineutral stationary model has been shown to be very useful in analyzing the physics of SPT operation thanks to a short time of calculation. In spite of the simplicity of the model, the numerical results are in good agreement with the experimental data. An important ingredient for this successful agreement is the introduction of a heuristic fading function of the wall-electron interactions outside the SPT channel. This approximation will be validated by future 2D simulations.

[1] A. I. Morozov, Y. V. Esipchuk, G. N. Tilinin, A. V. Trofimov, Y. A. Sharov, and G. Ya. Shshepkin, Sov. Phys. Tech. Phys. **17**, 38 (1972).

[2] D. H. Manzella, 30th AIAA/ASME/ASEE joint Propulsion Conference, June 27–29, 1994, Indianapolis, IN, 1994.

[3] W. A. J. Hargus and M. A. Cappelli, 35th AIAA/ASME/ASEE Joint Propulsion Conference, June 20–24, 1994, Los Angeles, CA, 1999.

[4] M. Lyszyk, A. Cadiou, M. Dudeck, and J. P. Marque, 3rd International Conference on SpaceCraft Propulsion ICSP, Cannes, France, 2000.

[5] J. M. Fife, M. Matinez-Sanchez, and J. Szabo, 33rd AIAA Joint Propulsion Conference, Seattle, WA, 1997.

[6] J. M. Fife, Ph.D. thesis, MIT, 1998.

[7] D. B. Van Gilder and I. D. Boyd, 34th AIAA Joint Propulsion Conference, Cleveland, OH, 1998.

[8] J. Bareilles, L. Garrigues, and J. P. Bœuf, in Ref. 4.

[9] J. P. Boeuf, L. Garrigues, and L. C. Pitchford, *Electron Kinetics and Applications of Glow Discharges* (Plenum, New York, 1998).

[10] L. Garrigues and J. P. Boeuf, J. Appl. Phys. **84**, 3541 (1998).

[11] N. B. Meezan, W. A. Hargus, and M. A. Cappelli, Phys. Rev. E **63**, 026410 (2001).

[12] F. Chen, *Introduction to Plasma Physics and Controlled Fusion* (Plenum, New York, 1984).

[13] S. Roche, Ph.D. thesis Dissertation, Orsay, France, 2001.

[14] S. Béchu, N. Gascon, S. Roche, M. Prioul, L. Albarede, P. Lasgorceix, and M. Dudeck, 36th Joint Propulsion Conference, AIAA-2000-3524, Huntsville, AL, July, 2000.

[15] M. Day, V. Kim, V. Kozlov, A. Lazurenko, G. Popov, and A. Skrylnikov, 25th International Electric Propulsion Conference, Cleveland, OH, 1997.